Title: Disc Antenna Enhanced Infrared Spectroscopy: From Self-Assembled Monolayers to Membrane Proteins

Author(s): Pfitzner, E., Seki, H., Schlesinger, R., Ataka, K., & Heberle, J.

Document type: Postprint

Disc Antenna Enhanced Infrared Spectroscopy: From Self-Assembled Monolayers to Membrane Proteins

[1]Emanuel Pfitzner, [1,2]Hirofumi Seki, [3]Ramona Schlesinger, [1]Kenichi Ataka, and [1]Joachim Heberle*

[1]Experimental Molecular Biophysics, Dept. of Physics, Freie Universität Berlin, Arnimalle 14, 14195 Berlin, Germany

[2]Toray Research Center Inc., 3-3-7 Sonoyama, Otsu, Shiga 520-8567, Japan

[3]Genetic Biophysics, Dept. of Physics, Freie Universität Berlin, Arnimalle 14, 14195 Berlin, Germany

ABSTRACT: Plasmonic surfaces have emerged as a powerful platform for biomolecular sensing applications and can be designed to optimize the plasmonic resonance for probing molecular vibrations at utmost sensitivity. Here, we present a facile procedure to generate metallic micro disc antenna arrays that are employed in surface-enhanced infrared absorption (SEIRA) spectroscopy of biomolecules. Transmission electron microscopy (TEM) grids are used as shadow mask deployed during physical vapor deposition of gold. The resulting disc-shaped antennas exhibit enhancement factors of the vibrational bands of 4×10^4 giving rise to a detection limit < 1 femtomol (10^{-15} mol) of molecules. Surface-bound monolayers of 4-mercaptobenzoic acid show polyelectrolyte behavior when titrated with cations in the aqueous medium. Conformational rigidity of the self-assembled monolayer is validated by density functional theory calculations. The membrane protein sensory rhodopsin II is tethered to the disc antenna arrays and is fully functional as inferred from the light-induced SEIRA difference spectra. As an advance to previous studies, the accessible frequency range is improved and extended into the fingerprint region.

Surface-enhanced infrared absorption spectroscopy (SEIRAS) has evolved from *in-situ* studies of molecules at electrified interfaces[1] to those of biological interest[2]. Most relevant to biomembrane research is the ability to detect monolayers of adsorbed molecules. Herein, conformational changes of membrane proteins in surface-tethered systems have been resolved,[3-9] the folding reaction of membrane proteins has been traced[10-11] and protein-protein interactions have been monitored by SEIRAS.[3, 12]

In a typical SEIRAS experiment, a rough gold film is deposited on a silicon prism and IR spectra are recorded in attenuated total reflection (ATR) geometry.[13] Although this method is well established, the enhancement of the infrared (IR) absorption bands is not very reproducible mainly due to variations in the experimental conditions during the formation of the rough metal surface (e.g. evaporation vs. chemical deposition, thickness, substrate roughness, deposition time etc.).[13-14] The workflow is hardly parallelizable due to the high cost of commonly used thick silicon prisms which reduce transmitted power and induce artifacts for frequencies < 1500 cm^{-1} due to the occurrence of Si phonons and Si-O vibrations.[15-16]

To overcome these limitations and to boost the signal-to-noise ratio in absorbance from surface adsorbed molecules, the use of metal antennas periodically arranged on CaF_2 whose collective plasmonic oscillations are coupled to molecular vibrations of interest, are highly promising.[17-18] Geometry, size, and arrangement of metal structures determine their plasmonic resonances.[18-22] Furthermore, the spectral separation of the plasmonic resonance and molecular vibrations of surface-bound molecules govern the resulting absorbance signal.[12, 22-26]

The recent years have witnessed enormous progress in understanding and controlling the plasmonic properties of the metal surfaces used for surface enhancement.[27] Gold antenna arrays with tailored geometries are generated by electron beam lithography (EBL),[17, 24] focused ion beam (FIB) milling,[28] laser-interference lithography (LIL)[29-31] or direct laser writing (DLW).[22] These methods typically require high-level infrastructure and long processing times for large areas (except for LIL). Another disadvantage is the use of electron- or photoresists, respectively, which need to be removed after metal deposition, thus, adding processing steps and potential precontamination to the antennas.

As an alternative to these methods, nanostencil lithography (NSL)[32-34] was successfully applied as a contact-free method for the reproducible production of structured gold surfaces for SEIRAS.[35] Still, the production of stencils is complicated and often requires expensive EBL dry etching equipment.[35] Here, we introduce a facile methodology for high-throughput and cheap production of structured gold surfaces by employing commercially available grids used for cryogenic transmission electron microscopy (TEM) as shadow mask during physical vapor deposition of gold.

Experimental Section

Preparation of Disc Antenna Arrays. Holey carbon film transmission electron microscopy (TEM) grids with aperture diameter of d = 2 μm and periodicity of p = 3 μm (2/1 C-Flat,

Protochips, Morrisville, USA) were attached to a CaF_2 slide ($\varnothing$ 13 mm, Eksma Optics, Vilnius, Lithuania), adhered with 1 μl of 2-propanol ($\geq$ 99.8 %, Carl Roth GmbH + Co. KG, Karlsruhe, Germany), and mounted in a homemade aluminum holder which provides tight attachment of the grid to the substrate. The grids were oriented such that the carbon film was averted from the substrate. In this geometry, the copper grid acts as a spacer between the carbon mask and the CaF_2 to prevent direct contact. The CaF_2 slides were sonicated in 2-propanol for 15 min, rinsed with milli-Q H_2O (resistivity: 18.2 MΩ cm^{-1}) and dried under ambient conditions prior to use. 50 nm of gold (99.999 % Au, Kurt J. Lesker Company Ltd., Hastings, England) were thermally evaporated in an EcoVap 3 Chamber (MBraun, Garching, Germany) at a rate of ~ 1 Å/s (p = 10^{-6} mbar). Samples were stored under N_2 or Ar atmosphere until use.

Preparation of 4-MBA SAM and pH Titration. Self-assembled-monolayers (SAM) of 4-MBA (99 %, Sigma-Aldrich Chemie GmbH, Munich, Germany) were established by immersing the antenna arrays for 1 h in 1 mM 4-MBA dissolved in water free DMSO (99 %, Sigma-Aldrich Chemie GmbH incubated with 4 Å molecular sieve, Sigma-Aldrich Chemie GmbH). For recording *in-situ* adsorption kinetics reflection spectra were recorded every 30 seconds (65 co-additions) while incubation with 1mM 4-MBA over 2 h. For the pH titrations the basin was rinsed with milli-Q H_2O and aqueous buffer (mix of 10 mM [sodiumcitrate + TRIS + PIPPS + CHES]) at different pH and NaCl concentrations were flushed through the flowcell. The pH of the buffer was adjusted by either 1M HCl (Carl Roth GmbH + Co. KG) or 1 M NaOH freshly prepared from dry pellets ($\geq$ 99 %, Carl Roth GmbH + Co. KG). The amount of acid or base added (~ 30 ml) for changing the pH of the buffer (~ 300 ml) increased the total NaCl concentration during the titration by up to 100 mM.

FTIR Spectroscopy on Disc Antenna Arrays. All spectroscopic measurements on disc antenna arrays were performed in external reflection mode on a Hyperion 2000 infrared microscope (Bruker, Ettlingen, Germany) equipped with a ×15, 0.4 NA Schwarzschild objective (angle of incidence: 10°-24°) and a mercury cadmium telluride (MCT) detector coupled to a Vertex 80v (Bruker) FTIR spectrometer. The field of view was limited to the size of an individual disc antenna array by blocking blades. The full width at half maximum (FWHM) of the objective was determined to $FWHM_x = 59 \pm 1$ μm, $FWHM_y = 64 \pm 1$ μm by scanning a gold edge across the focus in the absence of the blocking blades. 200-500 spectra were co-added at a mirror velocity of 40 kHz. All reflectance spectra are normalized against an unstructured, flat gold surface on the same substrate and smoothed (moving average filter with 5 points width, *Matlab R2015a*).

SEIRAS Spectroscopy Using Roughened Gold Surfaces. A thin gold film for silicon prism based SEIRAS was prepared by precipitation from a solution of $HAuCl_4$ as previously described.[36-37] A SAM of 4-MBA was generated by applying 1 mM 4-MBA dissolved in DMSO for 2 hours. All prism based SEIRA spectra were taken in a Vertex 70v FTIR spectrometer (Bruker) equipped with home-built optics.

Genetic Engineering and Production of the MACH-*Np*SRII-His. The transmembrane protein sensory rhodopsin II from *Natronomonas pharaonis* (*Np*SRII) was genetically engineered to introduce a MACH (methionine alanine cysteine histidine) sequence at the N-terminus. The sopII gene from *Np*SRII has been fused by polymerase chain reaction after a sequence coding for the four amino acids MACH and elongated with a coding sequence for 10 histidines for purification by Ni-NTA affinity chromatography. Thus, the resulting MACH-*Np*SRII protein has the flanking sequences: MACHMVGLTTLF.....HHHHHHHHHH. The new gene has been cloned under the control of the T7 promoter in pET15b (Amp^r; Invitrogen AG, Carlsbad, CA, USA), expressed in *Escherichia coli* BL21-CodonPlus (DE3) RP (Invitrogen) and purified essentially as described in.[38]

Surface-Tethering of Sensory Rhodopsin II and Light-Induced Difference SEIRAS. MACH-*Np*SRII is specifically bound to the gold surface via the terminal sulfhydryl group of the introduced cysteine residue. For all subsequent experiments, the disc antenna array was mounted in a custom flow cell whose bottom is a transparent CaF_2 window. A SAM of MACH-*Np*SRII solubilized in 0.05 % DDM (> 99 %, n-dodecyl-β-D-maltoside, Glycon Biochemicals GmbH, Luckenwalde, Germany), was established by incubation of the antennas for at least 6 h in buffer (50 mM MES, 4 M NaCl, pH 6.6) containing ~ 20 μg/ml *Np*SRII. A blue diode-pumped solid-state laser (473 nm, ~ 10 mW cm^{-2}, CNI, Changchun, China) excited *Np*SRII to accumulate the M state under photo-stationary conditions.[39] The presented spectra are averages of 4×10^5 individual spectra recorded at 8 cm^{-1} resolution on 4 different positions of a single disc antenna array. It is noted that the mirror speed was increased in these experiments to 240 kHz and the spectral range was limited to 2500 - 600 cm^{-1} with the help of a built-in optical filter to increase the rate of data recording.

Results and Discussion

Morphological and Spectroscopic Characterization

Square-shaped arrays (~ 90 × 90 μm^2) of gold discs with a nominal diameter of d = 2 μm, periodicity p = 3 μm (Figure 1a) and height of 50 nm were prepared on a total area of ~ 5 mm^2 (Figure 1b) as described (*vide supra*). Uniformity over individual squares was confirmed by visible microscopic images (Figure 1c) and topographically by atomic force microscopy (AFM, Figure 1d). Although the topography showed indistinct edges, optical microscopy through a ×15 Schwarzschild objective did not indicate any significant variations among different squares (except for some individual discs missing or squares totally covered by gold due to broken carbon films). For further spectroscopic analysis, only optically defect free arrays have been considered. Individual disc antenna arrays were spectroscopically characterized with an infrared microscope operating in reflection mode using top (antennas facing objective) and bottom (antennas averted from objective) configuration (Figure 2a). Each array consisted of approximately 900 disc antennas. Reflectance spectra of various disc antenna arrays were taken all over the substrate. Each array exhibits a plasmonic scattering peak at around 1800 cm^{-1}. The variation in the spectral shape on different locations on the sample can be attributed to edge blurring:[40] the finite size of the gold source during metal evaporation leads to a half-shadow, which smears out the resulting gold structures depending on the distance of the grid to the substrate (Figure S-1b-f). As a consequence, a redshift in the resonance energy is observed (Figure 2a, †) or the complete loss of the latter in cases where individual antennas are interconnected. A second

maximum arises at around 2250 cm^{-1} in all spectra. The multiple maxima in the spectra can be determined by applying grating theory due to the periodic arrangement of the disc antenna arrays: the used Schwarzschild objective illuminates and collects radiation under angles ranging from 10°-24° to the substrates normal.[28, 41] The collectively excited modes are shifted due to the momentum supplied by the grating. Here the amount of shift is determined by the angle of incidence. To scrutinize the shape of the observed reflectance spectrum by theory, we performed angle-resolved finite-difference time-domain (FDTD) simulations (cf. supporting information and Figure S-2). It is noted that according to literature[42] the disc antennas´ lateral aspect ratio of 1 is not expected to show the most efficient coupling to a vibrational mode of a bound molecule. In the framework of plasmonic scattering and plasmonic absorption, scattering dominates in our case.[42] Strong scattering is advantageous for the disc antenna arrays when employed in external reflection mode[12] since it leads to a higher number of collected photons.
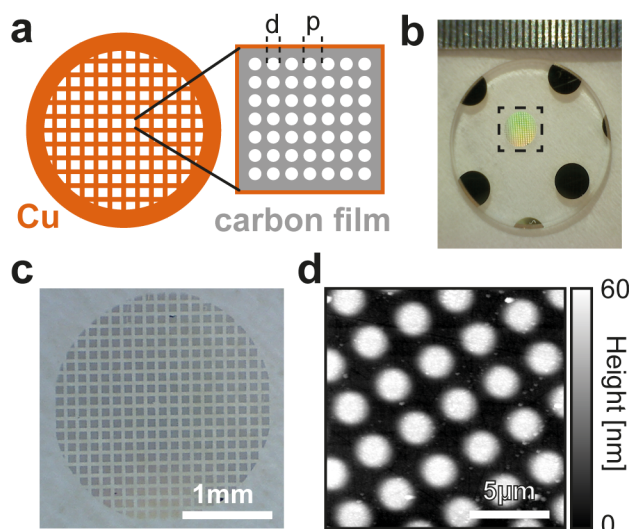
Figure 1. Microscopic and topographic characterization of the disc antenna arrays. (**a**) Sketch of the used TEM grids. The individual squares are ~ 90×90 µm^2 with the diameter of the apertures of d = 2 µm and a periodicity of p = 3 µm. (**b**) Photograph of a disc antenna array. The marked area is displayed in (**c**). The separation of the ticks on the scale corresponds to 0.5 mm. (**c**) Micrograph of the whole array (scale bar: 1 mm). (**d**) AFM topography of a disc antenna array (scale bar: 5 µm).

Surface-enhanced IR spectroscopy of tethered 4-mercaptobenzoic acid (4-MBA)

A self-assembled monolayer (SAM) was generated by binding the terminal sulfur of 4-MBA to the gold surface. As inferred from Figure 2a, the recorded vibrational spectrum of 4-MBA is overlaid by plasmonic scattering. Absorbance spectra were calculated by taking the negative logarithm of the reflectance before and after deposition of the SAM (Figure 2b).[12] It is evident by comparison to spectra recorded with ATR based SEIRAS (Figure 2b, blue trace) that the vibrational bands of 4-MBA when tethered to the disc antenna are identical (Table 1). The carbonyl stretching mode ν(C=O)[43] is shifted from 1683 cm^{-1} to 1712 cm^{-1} (dashed vertical lines) and exhibits a strong asymmetry which is also noted for the bulk ATR spectrum (Figure 2b, purple trace). The shift relates to a stronger hydrogen bonding via the network of carboxylic head groups

of 4-MBA.[44-45] The band asymmetry is attributed to different hydrogen-bonding conformations of the carboxylic head group.[46] The lower frequency modes at 1190 cm^{-1} and 1018 cm^{-1} [47] appear more intense than in the ATR spectrum. In comparison to conventional ATR based SEIRA spectroscopy, the contrast (by means of absorbance) in the disc antenna array spectra is approximately 5x larger and the usable spectral range spreads out to > 1000 cm^{-1} without any strong absorption of silicon phonons or silicon oxide. The often reported distorted Fano-line-shape[17, 48-50] of enhanced absorption bands is not observed in the spectra of our disc antenna arrays. The negative bands at 1263 cm^{-1} and 1108 cm^{-1} (labeled in Figure 2b by asterisks *) indicate contaminations by traces of poly(dimethylsiloxane)[51] that are replaced by the surface-bound 4-MBA. Coating the antennas with 4-MBA also increases the effective refractive index of the medium which results in a slight downshift of 5 cm^{-1} of the plasmonic resonance.[18, 52] As a consequence, a non-linear baseline (very broad, differential band shaped) is observed due to the high curvature of the plasmonic resonance spectrum at its maximum scattering frequency (~ 1800 cm^{-1}).[12] The reflection-absorption spectrum of an unstructured gold surface shows no detectable bands of adsorbed 4-MBA (Figure 2b, green trace).
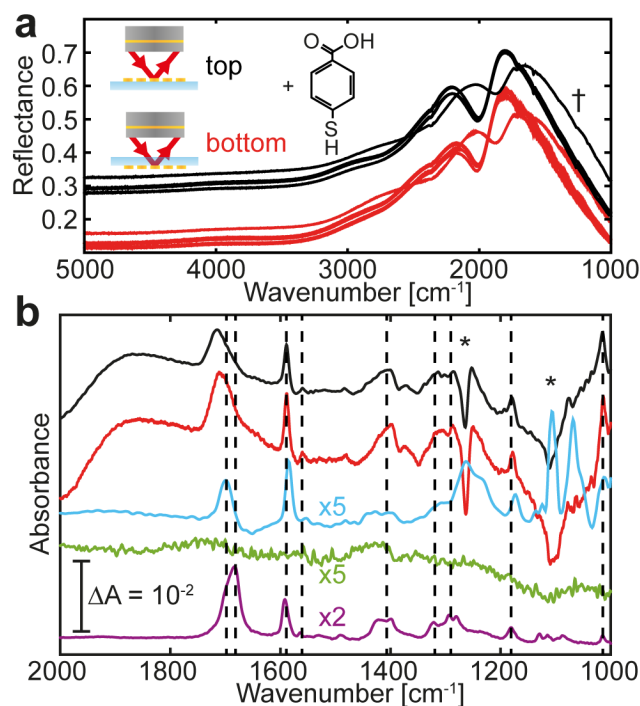
Figure 2. Spectroscopic characterization of the disc antenna arrays. (**a**) FTIR spectra of the disc antenna arrays after coating with a 4-MBA SAM in top (black trace) and in bottom configuration (red trace). Spectra have been recorded in external reflection mode. The significantly deviating spectra (†) have been recorded from the blurred array in Figure S-1d. (**b**) FTIR absorbance spectra after coating the disc antenna with 4-MBA (black and red traces), ATR-based SEIRA spectrum of surface-bound 4-MBA immersed in dimethylsulfoxide (DMSO) (blue trace), 4-MBA coated flat gold vs. uncoated flat gold (green trace) and bulk ATR spectrum of dry 4-MBA (purple trace). The asterisk denotes bands from poly(dimethylsiloxane).

Determination of the Enhancement Factor

To compare the herein presented substrates to previous work, we calculated the enhancement factor of the disc antenna array when immersed in DMSO and in dry environment according to published procedures (see supporting information).[24] We compare the apparent absorbance per molecule of four vibrational modes of the phenyl ring seen in the SEIRAS experiment with the absorbance per molecule derived from a dilution series of 4-MBA (in DMSO) in ATR configuration (Table 1, Figure S-3). The estimated enhancement factors of 4.5×10^4 in dry and 3.4×10^4 in DMSO are in the same order of magnitude as those reported in pervious SEIRAS studies in which EBL[18, 23, 53] or DLW[22] designed antennas with various geometries were employed.

Table 1. Vibrational assignment and enhancement factors for four vibrational modes associated to the phenyl ring.

ν_{DAA} [cm^{-1}][A]	ν_{ATR} [cm^{-1}][A]	ν_{DFT} [cm^{-1}] prot./deprot.	Assignment[B,47]	EF dry $\times 10^4$	EF DMSO $\times 10^4$
1589	1590	1626/1621	ν(C-C) (8a)	4.1	3.8
1559	1565	1592/1607	ν(C-C) (8b)	3.5	2.4
1190	1177	1180/1193	δ(C-H) (9a) or ν(C-O)	6.5	5.1
1018	1004	1028/1027	δ(C-H) (18a)	4.0	2.4

[A] in DMSO. [B] Wilson notation (in parenthesis) is used for the phenyl ring modes ν: stretching, δ: bending mode.

pH titration of a self-assembled monolayer of 4-mercapto-benzoic acid

We mounted the CaF$_2$ substrate in a home-built polytetrafluoroethylene (PTFE) flow cell (Figure 3a) to trace the adsorption kinetics of 4-MBA to the disc antennas.[12] Reflection difference spectra of a disc antenna array were acquired in bottom configuration. The formation of the SAM of 4-MBA was followed *in-situ* over two hours after the application of 1 mM 4-MBA dissolved in DMSO (Figure S-4). After exchange of the solvent DMSO to an aqueous buffer, the protonation state of the terminal carboxylic acid of 4-MBA (Figure 3b) was probed by pH titration. The flow-cell volume was exchanged by buffered solutions ranging from pH 3-11 (Figure 3c). Overall, the pH-induced difference spectra correspond well to spectra of 4-MBA SAMs recorded *ex-situ* by external reflection spectroscopy.[47] The intensity of the symmetric stretching vibration of the carboxylate moiety ν_s(COO$^-$) (~ 1400 cm^{-1}) and the C-O-H bending δ(C-O-H) (~ 1280 cm^{-1}) are plotted vs. pH in Figure 4a. Titrating the buffer in the absence of the SAM yielded negligible difference spectra (Figure S-5a). As expected for the deprotonation of the carboxylic acid head group, a decrease in absorbance of the ν(C=O) and δ(C-O-H) vibrational bands is observed while the ν_s(COO$^-$) of the corresponding carboxylate moiety is increasing. The transition spreads out over an extended pH range (between pH 3 and pH 10) and has its inflection point (pK$_a$) at around pH 6.5. The deviation of the data from the Henderson-Hasselbalch equation assuming a single protonation event (continuous lines in Figure 4a) illustrates the degree of broadening in the titration curve. Similar pH-dependent responses

were observed by surface-enhanced Raman spectroscopy.[54] Frequency upshift and line broadening of the carboxylic vibration are characteristic to polymeric acid behavior[55] and attributed to changes in the local electric field due to negatively charged carboxylates in close vicinity.[56] The upshift of the apparent pK$_a$ (about 2 pH units)[57] and broadening of the transition regime compared to carboxylic groups in solution agrees well with previous pH-dependent contact angle measurements of SAMs carrying carboxylates[56] and ATR-Fourier-Transformed Infrared (FTIR) spectroscopy of siloxane-anchored carboxylates.[58]
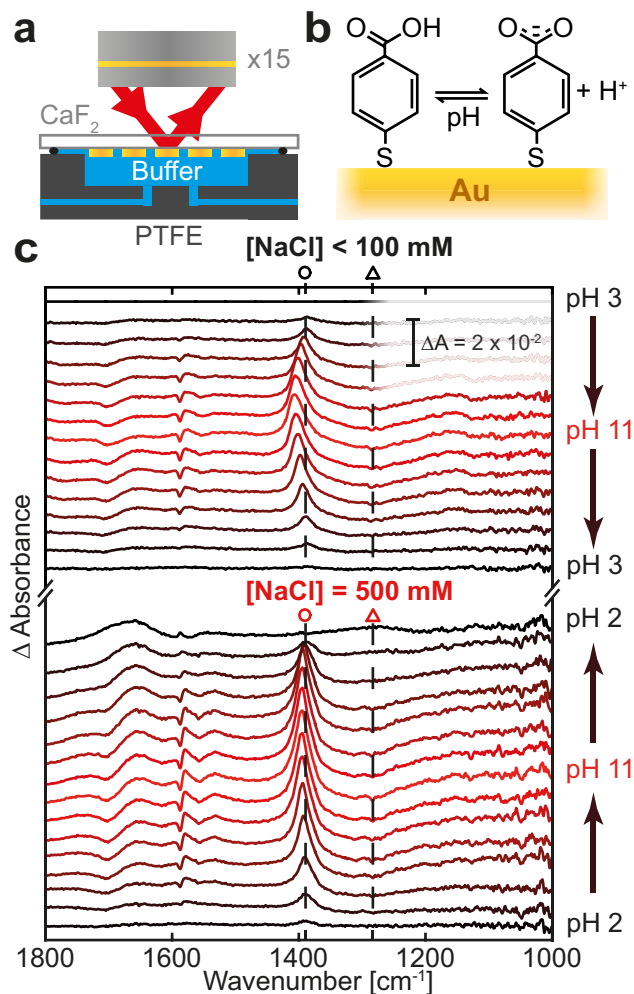
Figure 3. *In-situ* pH titration of a 4-MBA SAM. (**a**) Sketch of the flow-cell setup in plasmonic reflection mode. (**b**) pH-dependent protonation-state of 4-MBA. (**c**) Absorbance spectra during pH titration of adsorbed 4-MBA from pH 3(2) to pH 11 and back at [NaCl] < 100 mM and [NaCl] = 500 mM. For clarity, a smooth baseline was subtracted.

In addition to the increase in intensity of ν_s(COO$^-$) at elevated pH, a spectral shift to higher frequencies (Figure 4b) takes place at low salt concentration (Figure 3c, [NaCl] < 100 mM, the total concentration of NaCl increased during titration due to the addition of NaOH or HCl, respectively) which is reduced at higher salt concentration (Figure 3c, [NaCl] = 500 mM, cf. Figure S-5b). This shift has also been observed in earlier work on benzoic acid by potential-dependent SEIRAS and attributed to a change in dipole-dipole coupling upon reorientation.[59] To scrutinize this model we performed pH titrations at varying salt concentrations. The salt

dependence of the spectral shift of the $v_s(COO^-)$ vibration indicates that electrostatic shielding of the surface-bound negatively charged carboxylates are influenced by the presence of cations. To verify that only the frequency is salt dependent, we recorded SEIRA difference spectra of 4-MBA at various salt concentrations but constant pH (Figure S-5b). In addition to the spectral shift, the apparent pK_a is decreased by ~ 0.5 pH units at [NaCl] = 500 mM (Figure 4a). Qualitatively this effect can be understood by reducing the net electric field at the SAMs surface through increased charge screening at higher salt concentration. This observation has two implications: the lateral interaction (via hydrogen bonds) of the negatively charged carboxylate groups is suppressed which potentially leads to a down shift of its vibrational frequency. A decrease in the lateral electrostatic interaction reduces the probability of the (cooperative) deprotonation at a given pH which leads to a decreased apparent pK_a. Besides pH-induced difference bands originating from the carboxylic moiety ($v(C=O)$, $v_s(COO^-)$ and $\delta(C-O-H)$) there are difference bands in the range from ~ 1600 cm^{-1} to ~ 1500 cm^{-1}. Despite some ambiguity[43], most groups favor the assignment of the bands at 1589 cm^{-1} and 1559 cm^{-1} to the 8a and 8b ring modes, respectively.[47] Both modes exhibit a transition dipole moment along the phenyl ring which renders these marker bands for tracing the orientation of the aromatic ring versus the surface plane. To understand the origin of these difference bands, we performed density functional theory (DFT) calculations of 4-MBA in the protonated and in the deprotonated state in an aqueous environment (Figure S-6 and supporting information). It is noted that not all theoretically predicted vibrational modes are observed in the experimental spectra since only those vibrations are detected whose change in dipole moment has a component that is perpendicular to the plasmonic surface.[60] The calculations predict a 5x weaker intensity for the 8a mode as well as a downshift in frequency (Figure S-6) which could be observed as negative band at 1589 cm^{-1} and a positive band at 1578 cm^{-1} in the pH-induced difference spectra (Figures 3c and S-5a). The antisymmetric carboxylate stretching vibration $v_{as}(COO^-)$ couples to the 8b mode and, thus, splits up into two modes at ~ 1570 cm^{-1} and 1533 cm^{-1} (positive shoulder in difference spectra, Figures 3c and S-5a). The negative band at 1558 cm^{-1} can be accordingly assigned to a loss of 8b mode of the protonated state. Thus, a pH-induced reorientation of the SAM is disfavored over a purely vibrational rearrangement of the molecular modes. This finding is supported by the fact that any change in the tilt angle of 4-MBA relative to the surface normal should result in an increase of the $v_{as}(COO^-)$ band intensity.
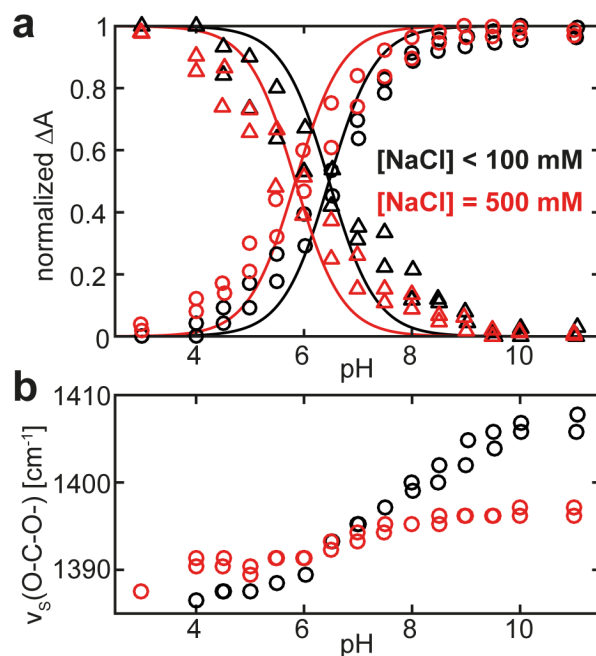
Figure 4. pH induced protonation state of the carboxylic moiety and shift of the related $v_s(COO^-)$ vibration. **(a)** Normalized absorbance of the $\delta(C-O-H)$ vibrational band at 1286 cm^{-1} (triangles) and the $v_s(COO^-)$ band at around 1400 cm^{-1} (circles) plotted vs. pH (see Figure 3c for color code) determined at < 100 mM NaCl and at 500 mM (black symbols). The Henderson-Hasselbalch equation (solid lines) has been fitted to the titration points. **(b)** Plot of the frequency of the symmetric stretching vibration of the carboxylate moiety ($v_s(COO^-)$ at ~ 1400 cm^{-1}) vs. solvent pH.

In-situ Adsorption of *Np*SRII-Proteins and Light-Induced Difference Spectroscopy

In an attempt to introduce the disc antenna arrays to biomembrane research, the membrane protein sensory rhodopsin II (from *Natronomonas pharaonis*, *Np*SRII) was tethered to the gold surface via a genetically engineered MACH-tag introduced to the N-terminus. The solvent exposed cysteine of the MACH-tag allows for efficient immobilization of the protein via its thiolate side chain. A monolayer of MACH-*Np*SRII, stabilized in detergent, was established (Figure S-7) and light-induced difference spectra were recorded (Figure 5a, red trace). Due to CaF$_2$ as substrate material, we were able to acquire light-induced SEIRA difference spectra in a range of 1100 - 1850 cm^{-1} which is of high diagnostic value (fingerprint region). Three negative bands at 1244 cm^{-1}, 1202 cm^{-1} and 1167 cm^{-1} evolve during illumination typical for the isomerized retinals $v(C-C)$.[39] The latter two agree with resonance Raman data and are indicative for an all-*trans*-configuration of the retinal.[61] The detection of small bands below 1100 cm^{-1} suffers from less plasmonic enhancement as well as deteriorated signal-to-noise ratio and, thus, will not be discussed any further. The strong negative band at 1545 cm^{-1} has been assigned to the $v(C=C)$ of all-*trans* retinal[39] that undergoes photo-isomerization to the 13-*cis* isomer. The difference bands between 1600 cm^{-1} and 1700 cm^{-1} are indicative for structural changes of the protein backbone. These are functionally relevant for signal transduction to the cognate transducer. The positive band at 1764 cm^{-1} originates from the $v(C=O)$ of the transiently protonated Asp 75.[39] All these features strongly

support the accumulation of an M-like state as previously reported and demonstrates functionality of the proteins, even under monolayer conditions.[60]
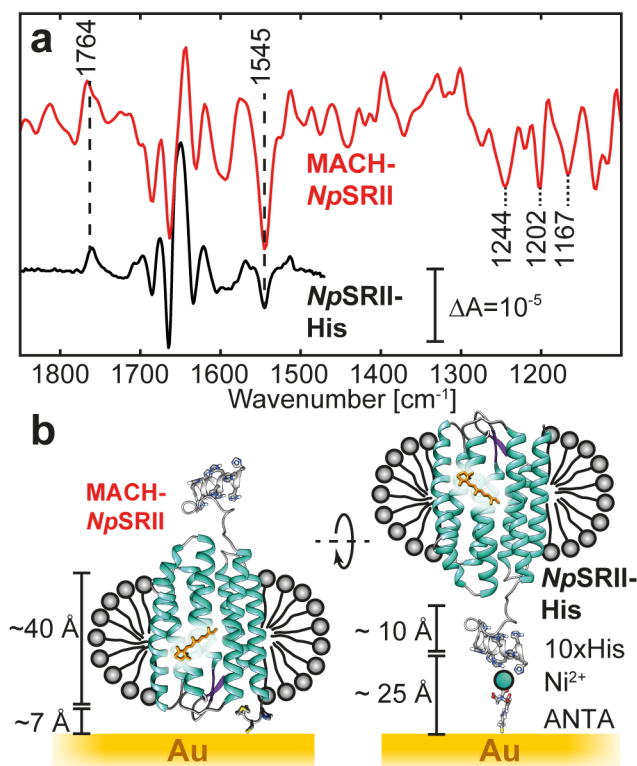
Figure 5. Light-induced difference spectroscopy of *Np*SRII. **(a)** Light-induced difference SEIRA spectra of monolayers of *Np*SRII immobilized via MACH-tag (red) or via His-tag (black, replotted from data published in [60] for comparison). **(b)** Schematic orientation of surface-tethered *Np*SRII via MACH or His-tag, respectively (PDB entry: 1JGJ[62], 10xHis-tag, MACH-tag and full-length C-terminus were modeled using Swiss-PDB viewer and visualized using the UCSF Chimera package[63]). Approximate distances from the gold surface are indicated.

The light-induced difference spectrum of *Np*SRII-His is shown for comparison which was immobilized via an oligo-histidine tag attached to a Nickel-nitrilo-triacetic acid linker SAM[3] (Figure 5a, black trace, replotted from).[60] As the His-tag is located at the C-terminus, the protein is tethered to the surface with the opposite orientation as with the MACH-tag (Figure 5b). It is evident that the signal-to-noise ratio is lower than of the ATR-SEIRA spectrum. This is owed to the fact that the disc antenna array spectra are recorded in a microspectroscopic setup, which has two implications. Firstly, the number of detected photons is reduced in reflection geometry which increases the noise level. Secondly, the amount of protein is approximately three to four orders of magnitude lower which affects the signal magnitude. Changing the thermal globar source to a brilliant light source (e.g. synchrotron radiation[64] or fiber-based IR laser[65]) can reduce the noise. Still, considering a gold surface (area 90 μm x 90 μm x 0.5, the latter factor considers the abundance of gold in the investigated region) that is fully covered by protein (area of protein: ~ 2 nm x 3 nm) we are able to detect < 1 femtomole of active membrane protein. Despite the limited spectral coverage in this experiment, the recorded vibrational bands in the two difference experiments are basically identical (Figure 5a) except for the relative intensity of the amide I and the ethyle-

nic retinal difference bands. This result is surprising considering the plasmonic field decays rapidly with the distance from the gold surface. We conclude that the orientational freedom of the *Np*SRII-His protein is expected to give rise to alterations in relative band intensities (Figure 5b).

Conclusion

We understand SEIRAS as an important tool in life sciences for acquisition of spectral data with a molecular level of detail at minute amounts of analyte. Thus, a facile, reproducible, and cheap method for preparation of SEIRAS substrates is in demand with their plasmon resonance frequency tuned to the range of 2000 - 1000 cm^{-1} where organic molecules exhibit characteristic vibrational fingerprints. We have investigated the morphology of these disc antenna arrays by visible and atomic force microscopy. The arrays have been employed in surface-enhanced IR microspectroscopic studies and enhancement factors of 4×10^4 have been found which allows for the detection of low quantities (sub-femtomoles) of molecules and their (bio-)chemical properties. The protonation state of the carboxylic moiety of a monolayer of 4-MBA was followed by *in-situ* SEIRAS. Comparison of the pH-dependent spectra with DFT calculations and literature suggests high rigidity of the 4-MBA SAM as well as electrostatically induced shifts of the symmetric carboxylate vibration. This spectral shift is significantly decreased at high salt concentration due to electrostatic screening of the negative charges of the SAM. As an application to biomembrane research, light-induced SEIRA difference spectra of the microbial rhodopsin *Np*SRII have been recorded. This work sets the basis for future spectroscopic investigation on solid-supported lipid bilayers. The latter span the disc antenna arrays and incorporate transmembrane proteins. Flowing receptor molecules across the bilayer with the help of a microfluidic system leads to binding-induced conformational changes, for example in a G-protein coupled receptor (GPCR),[66] which are detected by IR spectroscopy. The high sensitivity of the disc antenna approach is crucial for the application to proteins that can be produced in only low quantities.

ASSOCIATED CONTENT

Supporting Information

The Supporting Information is available free of charge on the ACS Publications website.

Supporting text including details on FDTD simulations, AFM study, enhancement factor calculation, ATR FTIR dilution series of 4-MBA, time evolution of the SAM adsorption and DFT calculations (PDF)

AUTHOR INFORMATION

Corresponding Author

* Prof. Dr. Joachim Heberle, email: Joachim.heberle@fu-berlin.de

Author Contributions

EP and HS conducted experiments. KA and JH designed experiments and essentially helped in interpreting the results. RS expressed and purified protein samples. EP and JH wrote the manuscript with contributions from all authors.

ABBREVIATIONS

AFM, atomic force microscope; ATR, attenuated total reflection; CHES, 2-(cyclohexylamino)ethanesulfonic acid; DFT, density functional theory; DDM, dodecyl-β-D-maltoside; DLW, direct laser writing; DMSO, dimethylsulfoxide; EBL, electron beam lithography; FDTD, finite-difference time domain; FIB, focused ion beam; FTIR, Fourier transform infrared; LIL, laser interference lithography; MES, 2-(4-morpholinyl)ethanesulfonic acid; *Np*SRII, sensory rhodopsin of *Natronomonas pharaonis*; NSL, nanostencil lithography; PIPPS, 3,3'-(1,4-piperazinediyl)di(1-propanesulfonic acid); PTFE, polytetrafluoroethylene; SAM, self-assembled monolayer; SEIRAS, surface-enhanced infrared absorption spectroscopy; TEM, transmission electron microscope; TRIS, 2-amino-2-(hydroxymethyl)-1,3-propanediol; 4-MBA, 4-mercaptobenzoic acid;

REFERENCES

(1)   Osawa, M., Dynamic Processes in Electrochemical Reactions Studied by Surface-Enhanced Infrared Absorption Spectroscopy (Seiras). *Bulletin of the Chemical Society of Japan* **1997,** *70*, 2861-2880.

(2)   Ataka, K.; Heberle, J., Electrochemically Induced Surface-Enhanced Infrared Difference Absorption (Seida) Spectroscopy of a Protein Monolayer. *Journal of the American Chemical Society* **2003,** *125*, 4986-4987.

(3)   Ataka, K.; Giess, F.; Knoll, W.; Naumann, R.; Haber-Pohlmeier, S.; Richter, B.; Heberle, J., Oriented Attachment and Membrane Reconstitution of His-Tagged Cytochrome C Oxidase to a Gold Electrode: In Situ Monitoring by Surface-Enhanced Infrared Absorption Spectroscopy. *Journal of the American Chemical Society* **2004,** *126*, 16199-16206.

(4)   Ataka, K.; Heberle, J., Biochemical Applications of Surface-Enhanced Infrared Absorption Spectroscopy. *Analytical and Bioanalytical Chemistry* **2007,** *388*, 47-54.

(5)   Ataka, K.; Stripp, S. T.; Heberle, J., Surface-Enhanced Infrared Absorption Spectroscopy (Seiras) to Probe Monolayers of Membrane Proteins. *Biochimica et Biophysica Acta (BBA) - Bioenergetics* **2013,** *1828*, 2283-2293.

(6)   Adato, R.; Aksu, S.; Altug, H., Engineering Mid-Infrared Nanoantennas for Surface Enhanced Infrared Absorption Spectroscopy. *Materials Today* **2015,** *18*, 436-446.

(7)   Fallah, M. A.; Stanglmair, C.; Pacholski, C.; Hauser, K., Devising Self-Assembled-Monolayers for Surface-Enhanced Infrared Spectroscopy of Ph-Driven Poly-L-Lysine Conformational Changes. *Langmuir* **2016,** *32*, 7356-7364.

(8)   Noguchi, H.; Adachi, T.; Nakatomi, A.; Yazawa, M.; Uosaki, K., Biofunctionality of Calmodulin Immobilized on Gold Surface Studied by Surface-Enhanced Infrared Absorption Spectroscopy: Ca^{2+}-Induced Conformational Change and Binding to a Target Peptide. *Journal of Physical Chemistry C* **2016,** *120*, 16035-16041.

(9)   Zhang, X. F.; Zeng, L.; Liu, L.; Ma, Z. F.; Jiang, X., Surface-Enhanced Infrared Absorption Spectroscopy and Electrochemistry Reveal the Impact of Nanoparticles on the Function of Protein Immobilized on Mimic Biointerface. *Electrochimica Acta* **2016,** *211*, 148-155.

(10)   Baumann, A.; Kerruth, S.; Fitter, J.; Buldt, G.; Heberle, J.; Schlesinger, R.; Ataka, K., In-Situ Observation of Membrane Protein Folding During Cell-Free Expression. *PloS One* **2016,** *11*, e0151051.

(11)   Harris, N. J.; Reading, E.; Ataka, K.; Grzegorzewski, L.; Charalambous, K.; Liu, X.; Schlesinger, R.; Heberle, J.; Booth, P. J., Structure Formation During Translocon-Unassisted Co-Translational Membrane Protein Folding. *Scientific Reports* **2017,** *7*, 8021.

(12)   Adato, R.; Altug, H., *In-Situ* Ultra-Sensitive Infrared Absorption Spectroscopy of Biomolecule Interactions in Real Time with Plasmonic Nanoantennas. *Nat Commun* **2013,** *4*, 2154.

(13)   Osawa, M.; Ataka, K., Electromagnetic Mechanism of Enhanced Infrared-Absorption of Molecules Adsorbed on Metal Island Films. *Surface Science* **1992,** *262*, L118-L122.

(14)   Enders, D.; Puccia, A., Surface Enhanced Infrared Absorption of Octadecanethiol on Wet-Chemically Prepared Au Nanoparticle Films. *Applied Physics Letters* **2006,** *88*, 2014-2017.

(15)   Chandler-Horowitz, D.; Amirtharaj, P. M., High-Accuracy, Midinfrared ($450cm^{-1} \leqslant \Omega \leqslant 4000cm^{-1}$) Refractive Index Values of Silicon. *Journal of Applied Physics* **2005,** *97*, 123526.

(16)   Johnson, F. A., Lattice Absorption Bands in Silicon. *Proceedings of the Physical Society of London* **1959,** *73*, 265-272.

(17)   Neubrech, F.; Pucci, A.; Cornelius, T. W.; Karim, S.; Garcia-Etxarri, A.; Aizpurua, J., Resonant Plasmonic and Vibrational Coupling in a Tailored Nanoantenna for Infrared Detection. *Physical Review Letters* **2008,** *101*, 157403.

(18)   Adato, R.; Yanik, A. A.; Amsden, J. J.; Kaplan, D. L.; Omenetto, F. G.; Hong, M. K.; Erramilli, S.; Altug, H., Ultra-Sensitive Vibrational Spectroscopy of Protein Monolayers with Plasmonic Nanoantenna Arrays. *Proceedings of the National Academy of Sciences of the United States of America* **2009,** *106*, 19227-19232.

(19)   Adato, R.; Artar, A.; Erramilli, S.; Altug, H., Engineered Absorption Enhancement and Induced Transparency in Coupled Molecular and Plasmonic Resonator Systems. *Nano Letters* **2013,** *13*, 2584-2591.

(20)   Hoffmann, J. M.; Yin, X.; Richter, J.; Hartung, A.; Maß, T. W. W.; Taubner, T., Low-Cost Infrared Resonant Structures for Surface-Enhanced Infrared Absorption Spectroscopy in the Fingerprint Region from 3 to 13 Mm. *The Journal of Physical Chemistry C* **2013,** *117*, 11311-11316.

(21)   Neubrech, F.; Beck, S.; Glaser, T.; Hentschel, M.; Giessen, H.; Pucci, A., Spatial Extent of Plasmonic Enhancement of Vibrational Signals in the Infrared. *ACS Nano* **2014,** *8*, 6250-6258.

(22)   Bagheri, S.; Weber, K.; Gissibl, T.; Weiss, T.; Neubrech, F.; Giessen, H., Fabrication of Square-Centimeter Plasmonic Nanoantenna Arrays by Femtosecond Direct Laser Writing Lithography: Effects of Collective Excitations on Seira Enhancement. *ACS Photonics* **2015,** *2*, 779-786.

(23)   Brown, L. V.; Zhao, K.; King, N.; Sobhani, H.; Nordlander, P.; Halas, N. J., Surface-Enhanced Infrared Absorption Using Individual Cross Antennas Tailored to Chemical Moieties. *Journal of the American Chemical Society* **2013,** *135*, 3688-3695.

(24)   Srajer, J.; Schwaighofer, A.; Ramer, G.; Rotter, S.; Guenay, B.; Kriegner, A.; Knoll, W.; Lendl, B.; Nowak, C., Double-Layered Nanoparticle Stacks for Surface Enhanced Infrared Absorption Spectroscopy. *Nanoscale* **2014,** *6*, 127-131.

(25)   Huck, C.; Toma, A.; Neubrech, F.; Chirumamilla, M.; Vogt, J.; De Angelis, F.; Pucci, A., Gold Nanoantennas on a Pedestal for Plasmonic Enhancement in the Infrared. *ACS Photonics* **2015,** *2*, 497-505.

(26)   Rezus, Y. L.; Selig, O., Impact of Local-Field Effects on the Plasmonic Enhancement of Vibrational Signals by Infrared Nanoantennas. *Optics Express* **2016,** *24*, 12202-12227.

(27)   Neubrech, F.; Huck, C.; Weber, K.; Pucci, A.; Giessen, H., Surface-Enhanced Infrared Spectroscopy Using Resonant Nanoantennas. *Chemical Reviews* **2017,** *117*, 5110-5145.

(28)   Mass, T. W. W.; Taubner, T., Incident Angle-Tuning of Infrared Antenna Array Resonances for Molecular Sensing. *ACS Photonics* **2015,** *2*, 1498-1504.

(29)   Xie, Q.; Hong, M. H.; Tan, H. L.; Chen, G. X.; Shi, L. P.; Chong, T. C., Fabrication of Nanostructures with Laser Interference Lithography. *Journal of Alloys and Compounds* **2008,** *449*, 261-264.

(30)   Liu, C. H.; Hong, M. H.; Cheung, H. W.; Zhang, F.; Huang, Z. Q.; Tan, L. S.; Hor, T. S., Bimetallic Structure Fabricated

by Laser Interference Lithography for Tuning Surface Plasmon Resonance. *Optics Express* **2008,** *16*, 10701-10709.

(31)   Bagheri, S.; Giessen, H.; Neubrech, F., Large-Area Antenna-Assisted Seira Substrates by Laser Interference Lithography. *Advanced Optical Materials* **2014,** *2*, 1050-1056.

(32)   Burger, G. J.; Smulders, E. J. T.; Berenschot, J. W.; Lammerink, T. S. J.; Fluitman, J. H. J.; Imai, S., High-Resolution Shadow-Mask Patterning in Deep Holes and Its Application to an Electrical Wafer Feed-Through. *Sensors and Actuators a-Physical* **1996,** *54*, 669-673.

(33)   Yan, X. M.; Contreras, A. M.; Koebel, M. M.; Liddle, J. A.; Somorjai, G. A., Parallel Fabrication of Sub-50-Nm Uniformly Sized Nanoparticles by Deposition through a Patterned Silicon Nitride Nanostencil. *Nano Letters* **2005,** *5*, 1129-1134.

(34)   Klemme, D. J.; Johnson, T. W.; Mohr, D. A.; Oh, S. H., Self-Aligned Grating Couplers on Template-Stripped Metal Pyramids Via Nanostencil Lithography. *Applied Physics Letters* **2016,** *108*, 213106.

(35)   Aksu, S.; Yanik, A. A.; Adato, R.; Artar, A.; Huang, M.; Altug, H., High-Throughput Nanofabrication of Infrared Plasmonic Nanoantenna Arrays for Vibrational Nanospectroscopy. *Nano Letters* **2010,** *10*, 2511-2518.

(36)   Ataka, K.; Heberle, J., Biochemical Applications of Surface-Enhanced Infrared Absorption Spectroscopy. *Anal. Bioanal. Chem.* **2007,** *388*, 47-54.

(37)   Osawa, M.; Ataka, K.; Yoshii, K.; Yotsuyanagi, T., Surface-Enhanced Infrared Atr Spectroscopy for in-Situ Studies of Electrode/Electrolyte Interfaces. *Journal of Electron Spectroscopy and Related Phenomena* **1993,** *64-5*, 371-379.

(38)   Radu, I.; Budyak, I. L.; Hoomann, T.; Kim, Y. J.; Engelhard, M.; Labahn, J.; Buldt, G.; Heberle, J.; Schlesinger, R., Signal Relay from Sensory Rhodopsin I to the Cognate Transducer Htri: Assessing the Critical Change in Hydrogen-Bonding between Tyr-210 and Asn-53. *Biophysical Chemistry* **2010,** *150*, 23-28.

(39)   Engelhard, M.; Scharf, B.; Siebert, F., Protonation Changes During the Photocycle of Sensory Rhodopsin Ii from *Natronobacterium Pharaonis*. *FEBS Letters* **1996,** *395*, 195-198.

(40)   Vazquez-Mena, O.; Villanueva, G.; Savu, V.; Sidler, K.; van den Boogaart, M. A.; Brugger, J., Metallic Nanowires by Full Wafer Stencil Lithography. *Nano Letters* **2008,** *8*, 3675-3682.

(41)   Liberman, V.; Adato, R.; Mertiri, A.; Yanik, A. A.; Chen, K.; Jeys, T. H.; Erramilli, S.; Altug, H., Angle-and Polarization-Dependent Collective Excitation of Plasmonic Nanoarrays for Surface Enhanced Infrared Spectroscopy. *Optics Express* **2011,** *19*, 11202-11212.

(42)   Neuman, T.; Huck, C.; Vogt, J.; Neubrech, F.; Hillenbrand, R.; Aizpurua, J.; Pucci, A., Importance of Plasmonic Scattering for an Optimal Enhancement of Vibrational Absorption in Seira with Linear Metallic Antennas. *Journal of Physical Chemistry C* **2015,** *119*, 26652-26662.

(43)   Li, R.; Lv, H.; Zhang, X.; Liu, P.; Chen, L.; Cheng, J.; Zhao, B., Vibrational Spectroscopy and Density Functional Theory Study of 4-Mercaptobenzoic Acid. *Spectrochimica Acta. Part A: Molecular and Biomolecular Spectroscopy* **2015,** *148*, 369-374.

(44)   Davey, R. J.; Dent, G.; Mughal, R. K.; Parveen, S., Concerning the Relationship between Structural and Growth Synthons in Crystal Nucleation: Solution and Crystal Chemistry of Carboxylic Acids as Revealed through Ir Spectroscopy. *Crystal Growth & Design* **2006,** *6*, 1788-1796.

(45)   Hadzi, D.; Sheppard, N., The Infra-Red Absorption Bands Associated with the Cooh and Cood Groups in Dimeric Carboxylic Acids. I. The Region from 1500 to 500 Cm^{-1}. *Proceedings of the Royal Society A: Mathematical, Physical and Engineering Sciences* **1953,** *216*, 247-266.

(46)   Rosendahl, S. M.; Burgess, I. J., Electrochemical and Infrared Spectroscopy Studies of 4-Mercaptobenzoic Acid Sams on Gold Surfaces. *Electrochimica Acta* **2008,** *53*, 6759-6767.

(47)   Wells, M.; Dermody, D. L.; Yang, H. C.; Kim, T.; Crooks, R. M.; Ricco, A. J., Interactions between Organized, Surface-Confined Monolayers and Vapor-Phase Probe Molecules. 9. Structure/Reactivity Relationship between Three Surface-Confined

Isomers of Mercaptobenzoic Acid and Vapor-Phase Decylamine. *Langmuir* **1996,** *12*, 1989-1996.

(48)   Luk'yanchuk, B.; Zheludev, N. I.; Maier, S. A.; Halas, N. J.; Nordlander, P.; Giessen, H.; Chong, C. T., The Fano Resonance in Plasmonic Nanostructures and Metamaterials. *Nat Mater* **2010,** *9*, 707-715.

(49)   Giannini, V.; Francescato, Y.; Amrania, H.; Phillips, C. C.; Maier, S. A., Fano Resonances in Nanoscale Plasmonic Systems: A Parameter-Free Modeling Approach. *Nano Letters* **2011,** *11*, 2835-2840.

(50)   Lahiri, B.; McMeekin, S. G.; De la Rue, R. M.; Johnson, N. P., Enhanced Fano Resonance of Organic Material Films Deposited on Arrays of Asymmetric Split-Ring Resonators (a-Srrs). *Optics Express* **2013,** *21*, 9343-9352.

(51)   Cai, D. K.; Neyer, A.; Kuckuk, R.; Heise, H. M., Raman, Mid-Infrared, near-Infrared and Ultraviolet-Visible Spectroscopy of Pdms Silicone Rubber for Characterization of Polymer Optical Waveguide Materials. *Journal of Molecular Structure* **2010,** *976*, 274-281.

(52)   Wu, C.; Khanikaev, A. B.; Adato, R.; Arju, N.; Yanik, A. A.; Altug, H.; Shvets, G., Fano-Resonant Asymmetric Metamaterials for Ultrasensitive Spectroscopy and Identification of Molecular Monolayers. *Nat Mater* **2011,** *11*, 69-75.

(53)   Huck, C.; Neubrech, F.; Vogt, J.; Toma, A.; Gerbert, D.; Katzmann, J.; Hartling, T.; Pucci, A., Surface-Enhanced Infrared Spectroscopy Using Nanometer-Sized Gaps. *ACS Nano* **2014,** *8*, 4908-4914.

(54)   Orendorff, C. J.; Gole, A.; Sau, T. K.; Murphy, C. J., Surface-Enhanced Raman Spectroscopy of Self-Assembled Monolayers: Sandwich Architecture and Nanoparticle Shape Dependence. *Analytical Chemistry* **2005,** *77*, 3261-3266.

(55)   Borukhov, I.; Andelman, D.; Borrega, R.; Cloitre, M.; Leibler, L.; Orland, H., Polyelectrolyte Titration: Theory and Experiment. *Journal of Physical Chemistry B* **2000,** *104*, 11027-11034.

(56)   Bain, C. D.; Whitesides, G. M., A Study by Contact-Angle of the Acid-Base Behavior of Monolayers Containing Ω-Mercaptocarboxylic Acids Adsorbed on Gold: An Example of Reactive Spreading. *Langmuir* **1989,** *5*, 1370-1378.

(57)   Brown, S. E.; Coates, J. H.; Duckworth, P. A.; Lincoln, S. F.; Easton, C. J.; May, B. L., Substituent Effects and Chiral Discrimination in the Complexation of Benzoic, 4-Methylbenzoic and (*Rs*)-2-Phenylpropanoic Acids and Their Conjugate Bases by *B*-Cyclodextrint and 6^a-Amino-6^a-Deoxy-*B*-Cyclodextrin in Aqueous Solution : Potentiometric Titration and ^{1}h Nuclear Magnetic Resonance Spectroscopic Study. *Journal of the Chemical Society-Faraday Transactions* **1993,** *89*, 1035-1040.

(58)   Cheng, S. S.; Scherson, D. A.; Sukenik, C. N., In-Situ Attenuated Total Reflectance Fourier-Transform Infrared-Spectroscopy of Carboxylate-Bearing, Siloxane-Anchored, Self-Assembled Monolayers: A Study of Carboxylate Reactivity and Acid-Base Properties. *Langmuir* **1995,** *11*, 1190-1195.

(59)   Han, B.; Li, Z.; Wandlowski, T., Adsorption and Self-Assembly of Aromatic Carboxylic Acids on Au/Electrolyte Interfaces. *Analytical and Bioanalytical Chemistry* **2007,** *388*, 121-129.

(60)   Jiang, X.; Zaitseva, E.; Schmidt, M.; Siebert, F.; Engelhard, M.; Schlesinger, R.; Ataka, K.; Vogel, R.; Heberle, J., Resolving Voltage-Dependent Structural Changes of a Membrane Photoreceptor by Surface-Enhanced IR Difference Spectroscopy. *Proceedings of the National Academy of Sciences of the United States of America* **2008,** *105*, 12113-12117.

(61)   Smith, S. O.; Braiman, M. S.; Myers, A. B.; Pardoen, J. A.; Courtin, J. M. L.; Winkel, C.; Lugtenburg, J.; Mathies, R. A., Vibrational Analysis of the *All-Trans*-Retinal Chromophore in Light-Adapted Bacteriorhodopsin. *Journal of the American Chemical Society* **1987,** *109*, 3108-3125.

(62)   Luecke, H.; Schobert, B.; Lanyi, J. K.; Spudich, E. N.; Spudich, J. L., Crystal Structure of Sensory Rhodopsin Ii at 2.4 Angstroms: Insights into Color Tuning and Transducer Interaction. *Science* **2001,** *293*, 1499-1503.

(63)   Pettersen, E. F.; Goddard, T. D.; Huang, C. C.; Couch, G. S.; Greenblatt, D. M.; Meng, E. C.; Ferrin, T. E., Ucsf Chimera—a Visualization System for Exploratory Research and Analysis. *Journal of Computational Chemistry* **2004,** *25*, 1605-1612.

(64)   Miller, L. M.; Dumas, P., Chemical Imaging of Biological Tissue with Synchrotron Infrared Light. *Biochimica et Biophysica Acta (BBA) - Bioenergetics* **2006,** *1758*, 846-857.

(65)   Gambetta, A.; Ramponi, R.; Marangoni, M., Mid-Infrared Optical Combs from a Compact Amplified Er-Doped Fiber Oscillator. *Optics Letters* **2008,** *33*, 2671-2673.

(66)   Ferrie, A. M.; Wang, C.; Deng, H.; Fang, Y., A Label-Free Optical Biosensor with Microfluidics Identifies an Intracellular Signalling Wave Mediated through the B$_2$-Adrenergic Receptor. *Integrative Biology: Quantitative Biosciences from Nano to Macro* **2013,** *5*, 1253-1261.

For TOC Only